Role of the different copper species on the activity of Cu/zeolite catalysts for SCR of NO$_x$ with NH$_3$

Unai De La Torre[1], Beñat Pereda-Ayo[1], Juan R. González-Velasco[1,*],

María José Illán-Gómez[2], Agustin Bueno-López[2].

[1]Departamento de Ingeniería Química, Facultad de Ciencia y Tecnología, Universidad del País Vasco, UPV/EHU, Campus de Leioa, P. O. Box 644, ES-48080 Bilbao, Bizkaia, Spain

[2]Department of Inorganic Chemistry. University of Alicante. Carretera de San Vicente s/n. E03080, Alicante (Spain)

Abstract

The SCR of NO$_x$ with NH$_3$ has been studied by using different Cu zeolite catalysts, prepared both with ZSM5 and BETA zeolite supports by ionic exchange or by impregnation. The catalysts were characterized by ICP-AES, N$_2$ adsorption at -196 ºC, XRD, TEM, XPS and H$_2$-TPR. The catalysts characterization confirmed the presence of different Cu(II) species on all catalyst (CuO and Cu(II) exchanged on tetrahedral and octahedral positions of the zeolites framework). Clear evidences of Cu(I) or Cu(0) species were not obtained. CuO was more abundant in high copper-content catalysts and in ZSM5 catalysts, due to its lower ionic exchange capacity, while isolated Cu(II) ions are more abundant in low copper-content catalysts and in BETA catalysts. It was concluded that CuO catalyzes the oxidation of NO to NO$_2$, and this favors the reduction of NO$_x$ at lower temperature (the NH$_3$-NO$_2$ reaction is faster than the NH$_3$–NO reaction because NO$_2$ is much more oxidizing than NO), whereas isolated Cu(II) ions maintain high NO$_x$ conversion at high temperatures.

Keywords: SCR, NO$_x$ removing, Cu-zeolite, Cu cluster

* Corresponding author:
Juan R. González-Velasco
Dept. Chemical Engineering
University of the Basque Country
P.O. Box 644, ES-48980 Bilbao, Spain
E-mail: juanra.gonzalezvelasco@ehu.es

1. Introduction

It is well recognized that the use of diesel and lean burn engines decreases the fuel consumption and thereby reduces the CO_2 emissions. However, conventional three way catalysts (TWC) are not capable to reduce nitrogen oxides (NO_x) from diesel engines due to the excess of oxygen in the exhaust. In the last decade, one of the main approaches proposed for NO_x reduction in diesel exhausts has been the selective catalytic reduction (SCR).

SCR was originally developed for stationary emission sources, mainly power plants [1]. However, it soon turned out to be a promising technology for the NO_x removal in automobile applications as well [2]. In 2005 it was introduced for commercial heavy-duty vehicles in Europe, and more recently also for passenger cars. The NH_3-SCR converter needs an external source of the selective reducing agent, e.g. urea. The urea solution is injected in a controlled way into the exhaust line, where it is thermally decomposed into NH_3 and CO_2. The ammonia then reacts selectively with NO_x under lean (oxidising) conditions, giving N_2 as the final product [3]. Non-noble metals like copper, iron and cerium supported on ZSM5 and BETA zeolite are among the most active catalysts for the urea/NH_3-SCR process [4-7], among others like copper/chabazite catalysts [8,9].

Cu(II) ion-exchanged ZSM5 (Cu-ZSM5) zeolites were first tested, showing high NO decomposition rates and NO_x SCR activities [10]. More recently, Cu(II)-exchanged BETA zeolites (Cu-BETA) have shown a good activity for the NH_3-SCR of NO_x, but they present better hydrothermal stability than similar ZSM5 catalysts [11]. Burch et at. [12] identified the presence of Cu(I) species under reaction conditions, and proposed that Cu(I) is the main active species for the reaction. Whatever, it is generally accepted that both copper ions (Cu(II) and/or Cu(I)), which exist in the exchange sites of ZSM5,

play an important role in the reaction of NH_3-SCR. In the last decade, a lot of research has been performed to obtain information about the nature of the copper active sites for this process [13-17].

Nevertheless, there is still an open discussion concerning the chemical and mechanistic aspects involved in SCR, mainly those related with the role of the different copper species exchanged or placed on the zeolite. In our previous work [18], we have analysed the NH_3-SCR catalytic performance of different ZSM5 and BETA supported catalysts, varying the preparation method and copper content. We found that while ZSM5 supported catalysts achieved better NO_x conversion in a low temperature range (250-350 °C), BETA supported catalysts were active at higher temperature (350-450 °C). On the other hand, an increase in the copper content and the use of an impregnation preparation method (vs. the ion exchange) allows achieving higher NO_x conversion at lower temperatures but it decreases at intermediate and higher temperatures.

The aim of this work is to understand the role of the different copper species on the activity of Cu/zeolite catalysts in the NH_3-SCR process for NO_x removal in a wide temperature range (140–500 °C). For characterization of the different Cu-zeolite catalysts, which were prepared by both impregnation and ion-exchange methods, XPS, H_2-TPR and TEM techniques have been used.

2. Experimental

2.1. Catalysts preparation.

The SCR catalysts consisted of copper-supported zeolites. Fresh zeolites were supplied by Zeolyst International, namely CP414E (BETA, Si/Al=12.5) and CBV5524G (ZSM5, Si/Al=25). The zeolites were first calcined at 550 ºC for 4 h to obtain the acid

form. The catalysts were prepared by two different conventional procedures: ion

exchange (IE) and wetness impregnation (IM). Metal ion exchange was carried out by

dissolving the required amount of $Cu(COOCH_3)_2$ (Panreac, 98%) in water. Then, H-

ZSM5 or H-BETA was added to this solution (8 g/L) and it was stirred for 24 h at 65 ⁰C.

The ion exchanged zeolites were then filtered, washed twice with deionized water,

dried overnight at 110 ⁰C and calcined at 550 ⁰C for 4 h.

On the other hand, the wetness impregnation method consisted of adding

slowly the required amount of the copper precursor dissolved in water (1.5 wt.%) at 40

⁰C and 3 mm Hg to 6 grams of H-BETA or H-ZSM5, under continuous rotation until the

solvent was evaporated. The samples were dried overnight at 110 ⁰C and calcined at

550 ⁰C for 4 h.

All the catalysts were then pelletized, crushed and sieved to 0.3-0.5 mm.

Previous experiments carried out with different particle size catalysts revealed that

mass transfer limitations were not controlling the reaction kinetics for a particle size of

0.3-0.5 mm.

The most relevant details of the preparation procedure of copper-zeolite

catalysts, as well as the nomenclature used are summarized in Table 1. For each

support, BETA or ZSM5, four catalysts were prepared, three by ion exchange and one

by wetness impregnation. With regards to the ion exchange catalysts, increasing

copper concentration solutions (160, 320, 640 and 2000 ppm) were used in order to

obtain different copper loading on the zeolitic support.

TABLE 1

2.2. Characterization techniques.

ICP-AES. The actual amount of copper in the prepared catalysts was determined by ICP-AES, after metal extraction from the solid samples with 1:2 HNO_3:HF mixture at 90 ºC, which assures complete samples dissolving.

N_2 adsorption. The BET surface area of the zeolite samples were determined by N_2 adsorption at −196 °C using a Micromeritics ASAP 2020 equipment.

XR Diffraction (XRD). The crystalline structure of the copper modified zeolite samples were analyzed by XRD (Philips PW1710 diffractometer). The samples were finely ground and X-Ray diffractograms were recorded with copper Kα radiation in continuous scan mode from 5 to 80° of 2θ with 0.02° per second sampling interval. PANalytical X'pert HighScore specific software was used for data treatment. JCPDS database was used to interpret the diffractograms.

X Ray Photoelectronic Spectroscopy (XPS). XPS characterization was carried out in a VG-Microtech Multilab electron spectromenter using Mg-Kα (1254.6 eV) radiation source. To obtain the XPS spectra, the pressure of the analysis chamber was maintained at $5 \cdot 10^{-10}$ mbar. The binding energy (BE) scale was adjusted by setting the carbon 1s transition at 284.6 eV. The XPS measurements were performed in the electron binding energy ranges corresponding to copper 2p, oxygen 1s, silicon 2p, aluminum 2p and carbon 1s core excitations [19, 20].

Transmission Electron Microscopy (TEM). A JOEL (JEM-2010) microscope was used to obtain TEM images of the catalysts. Few droplets of an ultrasonically dispersed suspension of each sample in ethanol were placed on a copper grid with lacey carbon film and dried at ambient conditions for TEM characterizations. In order to obtain particle size distribution of copper, around 200 copper particles were identified and measured.

140   *Hydrogen Temperature Programmed Reduction (H_2-TPR).* Reducibility of

141   copper catalysts was investigated by TPR using H_2. The samples were pretreated in 30

142   ml/min of 10% O_2/He mixture gas flow at 550 ºC for 45 min and then cooled down to 30

143   ºC and flushed out with helium for 60 min. Then the samples were heated from room

144   temperature to 600 ºC with 10 °C/min ramp in a 60 ml/min of 5% H_2/Ar mixture gas

145   flow. The water formed during reduction with H_2 was trapped using a cold trap and the

146   hydrogen consumption was continuously monitored with a TCD detector.

147

148   *2.3. SCR experiments.*

149   The SCR experiments were performed in a down flow stainless steel reactor.

150   The reactor tube, with 1 g of 0.3-0.5 mm pelletized Cu-zeolite SCR catalyst inside, was

151   located into a 3-zone tube furnace. The temperature was measured by a thermocouple

152   at the top of the catalyst bed. The reaction temperature was varied from 100 to 500 ºC

153   in steps of 40 ºC. The composition of the feed gas mixture was 750 ppm NO, 750 ppm

154   NH_3 and 9.5% O_2 using Ar as the balance gas. Gases were fed via mass flow

155   controllers and the total flow rate was set at 3000 ml·min^{-1}, which corresponded to a

156   space velocity (GHSV) of 90,000 h^{-1}. The experimental set-up was designed to

157   minimize the gas phase oxidation of NO to NO_2, and therefore, the NO_2 concentration

158   in the gas fed is almost null. The NO, NO_2 NH_3 and N_2O concentrations at the reactor

159   exit were monitored every 40 ºC, once the analysis has been stabilized for at least 10

160   min, by an online FTIR multigas analyzer (MKS 2030).

161   The NO (X_{NO}) and NH_3 (X_{NH3}) conversions were calculated as

162
$$X_{NO} = \frac{F_{NO}^{in} - F_{NOx}^{out}}{F_{NO}^{in}} \times 100 \qquad (1)$$

163
$$X_{NH_3} = \frac{F_{NH_3}^{in} - F_{NH_3}^{out}}{F_{NH_3}^{in}} \times 100 \qquad (2)$$

164　　and the N_2 (S_{N2}), NO_2 (S_{NO2}) and N_2O (S_{N2O}) selectivities were calculated as

165
$$S_{N_2} = \frac{2F_{N_2}^{out}}{F_{NH_3}^{in}X_{NH_3}+F_{NO}^{in}X_{NO}} \times 100 \qquad (3)$$

166
$$S_{NO_2} = \frac{F_{NO_2}^{out}}{F_{NH_3}^{in}X_{NH_3}+F_{NO}^{in}X_{NO}} \times 100 \qquad (4)$$

167
$$S_{N_2O} = \frac{2F_{N_2O}^{out}}{F_{NH_3}^{in}X_{NH_3}+F_{NO}^{in}X_{NO}} \times 100 \qquad (5)$$

168　　where F_i represents the concentration of the "i" specie and the superscripts "in" and

169　　"out" indicate that the gas concentration was measured at the inlet and the exit of the

170　　reactor, respectively.

171

172　　**3. Results and Discussion.**

173　　*3.1 Analysis of the copper content and surface area of the catalysts.*

174　　　　Figure 1 shows the copper loading of the different catalysts prepared by ionic

175　　exchange with regard to the initial copper concentration on the water solutions used for

176　　the exchange process. An auxiliary continuous line has been included which

177　　represents the maximum copper loading that would be achieved if all copper available

178　　in the water solutions were incorporated into the zeolites. Furthermore, two auxiliary

179　　dot lines represent the maximum amount of copper that can be exchanged on each

180　　zeolite. The Si/Al ratios and the corresponding molecular composition of the ZSM5 and

181　　BETA zeolites (Table 1) predict these maxima amounts of copper are 2 and 5.6 wt. %,

182　　respectively, considering that one Cu(II) cation needs two ionic exchange sites.

183　　　　　　　　　　　　　　　　FIGURE 1

184　　　　All data on Figure 1 lie below the concentration predicted by the auxiliary

185　　continuous line corresponding to maximum copper loading, evidencing that there is

186   copper left in the water solutions after the exchange processes. The amount of copper

187   loaded on both zeolites increases with copper concentration in the water solution, and

188   as a general trend, the amount of copper loaded on the ZSM5 zeolite is lower to that

189   loaded on BETA zeolite (for similar exchange conditions). This is in agreement with the

190   Si/Al ratios and with the exchange capacity of each zeolite. The copper loading on the

191   BETA zeolite catalysts increases with the copper concentration on the water solution

192   until total consumption of the exchange sites on the B-IE-5.8 catalyst. On the contrary,

193   some Cu-ZSM5 catalysts exceed the 100 % exchange level, and this can be due either

194   to the formation of copper dimers in solution $(Cu^{2+}OH^-)_2$, which would result in the

195   anchoring of two Cu(II) ions per exchangeable site [21], and/or to the formation of

196   extraframework copper species. During the ion exchange, local changes in pH could

197   promote copper hydroxide precipitation [22].

198   In spite of this observation, the X ray diffractograms of the copper-exchanged

199   zeolites, which are not shown for the sake of brevity, did not present neither peaks

200   corresponding to metallic copper (Cu^0) nor to copper oxide (CuO), evidencing high

201   copper dispersion in all cases. Besides, the diffractograms of the acid and copper

202   exchanged zeolites are quite similar, which means that the crystalline structure of the

203   zeolites was not apparently modified after the copper incorporation.

204   Figure 2 shows the BET surface area of the catalysts as a function of the

205   copper loading. Fresh BETA and ZSM5 zeolites presented BET surface areas of 532

206   and 474 $m^2 \cdot g^{-1}$, respectively. These areas decrease linearly, with almost the same

207   slope, with the copper content. This decrease of BET surface area can be attributed to

208   the partial pores blockage by copper species and/or to the destruction of micropores

209   during copper loading due to aluminum leaching by acid attack [23]. The surface area

210   decrease observed for the impregnated catalysts (B-IM-1.3 and Z-IM-1.2) are not in

211   line with their counterparts prepared by ion-exchange, and impregnated catalysts show

212 a much higher decrease in the BET surface area. This suggests that pore blockage by

213 copper species is the main reason of the BET surface area decrease.

214   FIGURE 2

215

216 *3.2 Analysis of the copper particle size by TEM.*

217   The copper particle size distributions on the different catalysts have been

218 determined by TEM. As an example, Figures 3a and 3b show TEM images of the

219 lowest and highest copper content ZSM5 catalysts, whereas Figures 3c and 3d show

220 the counterpart BETA catalysts, all of them prepared by ionic exchange.

221   FIGURE 3

222   As expected, the amount and size of the dark spots, mainly attributed to CuO as

223 it will be demonstrated afterwards, depends both on the nature of the zeolite and on the

224 copper loading. A major number of dark spots are observed for high-copper content

225 catalysts (Z-IE-4.9 and B-IE-5.8, Figures 3b and 3d) than for the counterpart low-

226 copper content catalysts, and BETA catalysts only shows small particles (diameter <

227 1.5 nm) while ZSM5 presents both small and large particles.

228   Figure 4 shows the copper particle size distribution for all catalysts. No relevant

229 differences were detected in the copper size distribution among catalysts prepared by

230 impregnation and ionic exchange.

231   FIGURE 4

232   As a general trend, BETA catalysts present narrower particle size distribution

233 than ZSM5 catalysts, with particle sizes centered on 1 nm and most particles being

234 smaller than 4 nm. Only the highest-copper content BETA catalyst (B-IE-5.8) shows

235 few copper particles larger than 10 nm. ZSM5 catalysts exhibit wider particle size

236   distributions than BETA catalysts, and a considerable amount of large particles,

237   especially for high copper loading catalyst, were identified. Few of these particles

238   achieved sizes even higher than 300 nm.

239   These observations are in good agreement with the conclusions of the previous

240   section, where it was observed that copper is mainly exchanged on zeolite sites of the

241   BETA support while an important fraction of the metal loaded on ZSM5 is impregnated

242   rather than exchanged (see Figure 1 and previous section). These differences are

243   consistent with the Si/Al ratio and ionic exchange capacity of both zeolites. However, it

244   is important to pay especial attention to the Z-IE-1.4 sample, since large CuO particles

245   are observed in the TEM images but the total ionic exchange capacity has not been

246   achieved (see Table 1). This suggests that not only the ionic exchange capacity (or the

247   Si/Al ratio) of the zeolites plays a role on the nature of the copper species formed, but

248   also the zeolite structure seems to be involved. The framework types of the BETA and

249   ZSM5 zeolites are BEA and MFI, respectively, and the accessible volumes of these

250   structures are 23 and 10 % respectively [24]. Also, the maximum diameter of a sphere

251   that can enter into these structures is 6.68 Å for BEA and 6.36 Å for MFI. According to

252   this, the copper solution used for the ionic exchange is expected to enter more easily

253   into the BETA zeolite porosity than on the ZSM5 porosity, and therefore, a smaller

254   particle size distribution of the CuO particles is obtained in the BETA zeolite catalysts.

255

256   *3.3 Analysis of the copper species nature by XPS and H_2-TPR.*

257   In order to study the surface composition of the catalysts and the nature of the

258   surface copper species, XPS characterization was carried out. A certain amount of

259   carbon was detected by XPS on the surface of all catalysts, close to 10% in some

260   cases, and for this reason a direct analysis of the quantitative results of the surface

261 composition is complex and comparison of elements ratio is more meaningful. In Table

262 2, the Si/Al surface ratios are compiled together with the ratio between surface copper

263 (determined by XPS) and total copper (determined by ICP) contents.

264   TABLE 2

265   The Si/Al surface ratio decreases by increasing the copper loading both for

266 BETA and ZSM5 catalysts. This can be attributed to the decrease of the solutions pH

267 by increasing the Cu(II) precursor concentration, which favors the zeolites

268 dealumination [23]. This aluminum leaching would result in a certain accumulation of

269 aluminum species on the crystals surface.

270   The ratio between surface and total copper contents ($Cu_{surface}/Cu_{total}$) provides

271 information about the metal loading process. Constant ratios (0.42) were obtained for

272 BETA zeolite catalysts prepared by ionic exchange and a quite similar value was

273 obtained by impregnation of this support (0.37 for B-IM-1.3). These values below 1

274 indicate that copper is mainly accumulated into the zeolite porosity, and support that

275 copper cations are actually exchanged on the zeolite sites [25]. The similar values

276 obtained by the impregnation and ionic exchange loading methods suggest that copper

277 could be exchanged even in the impregnated BETA catalyst. For ZSM5 catalysts

278 prepared by ionic exchange, the $Cu_{surface}/Cu_{total}$ ratio increases with the copper loading

279 and most values are higher than those obtained with the counterpart BETA zeolite

280 catalysts. This is in line with the worst copper dispersion obtained on the ZSM5 zeolite

281 support. Note that higher particles were observed by TEM on ZSM5 zeolite catalysts

282 (see Figures 3 and 4). This worst dispersion of copper can be attributed to the higher

283 Si/Al ratio, and therefore lower cation exchange capacity, of the ZSM5 zeolite with

284 regard to that of the BETA zeolite and to the more accessible porosity of the BETA

285 zeolite. The $Cu_{surface}/Cu_{total}$ ratio obtained with the ZSM5 zeolite impregnated with

11

286   copper (Z-IM-1.2 catalyst) is higher than values obtained by ionic exchange of this

287   zeolite, which is an evidence of worst dispersion in this case.

288   Figures 5a and 5b show the X ray photoelectronic spectra corresponding to the

289   copper 2p transition for Cu-ZSM5 and Cu-BETA catalysts, respectively. It is usually

290   reported that Cu($2p^{3/2}$) transition appears at energy values lower than 933 eV for

291   metallic copper (Cu^0) and Cu$_2$O (Cu(I)), while it shifts to values higher than 933 eV for

292   Cu(II) species [26]. According to this assignation, all profiles included on Figure 5 are

293   consistent with the presence of different Cu(II) species. The presence of the shake-up

294   satellite (not shown in Figure 5) appearing in all catalysts with energies 10 eV higher

295   than the Cu($2p^{3/2}$) transition also gives evidences of the presence of Cu(II). However,

296   the energy of the Cu($2p^{3/2}$) transition does not allow unequivocally identify the oxidation

297   states of copper [23], and for the proper identification of the oxidation state of the

298   copper species the Auger peak must be taken into account. The Auger parameter (α),

299   which is calculated as the sum of copper 2p binding energy and Auger peak kinetic

300   energy, has been included in Table 3. The values of the Auger parameter of most

301   catalysts are well above 1850 eV, and these values confirm the presence of Cu(II)

302   cations. Only the Z-IE-4.9 catalyst presents Auger values below 1850 eV, and this

303   could be due to the formation of bulk CuO instead of Cu(II) cations exchanged on the

304   zeolite framework and/or to the presence of Cu(I) cations, but the formation of CuO

305   seems to be more reasonable [27].

306   TABLE 3

307   FIGURE 5

308   The Cu($2p^{3/2}$) transition included on Figure 5 can be deconvoluted in three main

309   contributions located around 933.2 eV, 934.0 eV and 936.0 eV. As discussed, all these

310   contributions can be most likely be attributed to different Cu(II) species [19]. The band

311   located at ca. 933.2 eV is tentatively assigned to agglomerated CuO particles present

312   on the surface [28], while second and third peaks located at ca. 934.0 and 936.0 eV

313   are thought to correspond to isolated Cu(II) species with different coordination, as was

314   evidenced by Hajjar et al. [29] by FTIR and MQMAS NMR. The peak at 934.0 eV

315   corresponds to isolated Cu(II) in tetrahedral coordination, while the peak appearing at

316   936.0 correspond to isolated Cu(II) in octahedrical coordination [28], which is related to

317   the presence of two kinds of exchange sites in the zeolites framework. As isolated

318   Cu(II) in octahedrical coordination are more strongly attached to the zeolite framework,

319   the corresponding contribution appears at the highest binding energy followed by

320   isolated Cu(II) in tetrahedral coordination and finally agglomerated Cu(II) species which

321   appear at the lowest binding energy.

322   The contribution of each individual transition to the total intensity of the Cu($2p^{3/2}$)

323   band depends both on the zeolite type and on the copper content. As a general trend,

324   increasing copper content leads to an increase in the contribution located at lowest

325   binding energy, i.e. 933.2 eV (dashed red line) to the detriment of that located at 934.0

326   eV (dashed green line), while the third one located at 936.0 eV (dashed blue line)

327   remains constant for Cu-ZSM5 and increases for Cu-BETA. The areas of these

328   contributions were calculated and expressed as a percentage of the total Cu($2p^{3/2}$)

329   transition in Table 3.

330   Note that the increasing contribution of the peak located at 933.2 eV, indicating

331   the presence of agglomerated CuO particles, increases with the copper loading: 13%

332   of the total Cu($2p^{3/2}$) transition for Z-IE-1.4, 31 % for Z-IE-2.6 and 53 % for Z-IE-4.9.

333   Meanwhile, the contribution of isolated Cu(II) in tetrahedral coordination shows a

334   reverse relationship respect to the amount of agglomerated particles, decreasing with

335   increasing the copper content, i.e. 78 % for Z-IE-1.4, 59 % for Z-IE-2.6 and 38 % for Z-

336   IE-4.9. The contribution of isolated Cu(II) in octahedrical coordination is almost
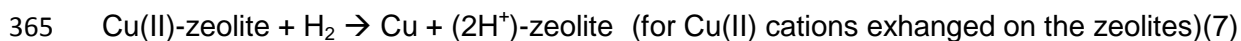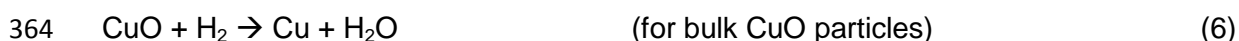
13

337   constant, around 9 %, regardless the copper loading. Thus, it can be suggested that

338   copper first preferentially occupies the ion exchange sites and, once those are

339   saturated, CuO is accumulated on the zeolite surface. Agglomerated CuO particles are

340   more abundant in ZSM5 zeolite than on BETA zeolite if catalysts with similar copper

341   loading are compared. For instance, the signal attributed to CuO particles represents

342   53 % in Z-IE-4.9 catalysts while it results in just 34 % for B-IE-5.8, although the copper

343   loading is even higher for the latter. This fact could be related to the higher Si/Al ratio,

344   and therefore lower cation exchange capacity, of the ZSM5 zeolite with regard to that

345   of the BETA zeolite and to the more accessible porosity of the BETA zeolite, which

346   promotes the formation of CuO aggregates for high copper loadings. Finally, XPS does

347   not show significant differences between ion exchanged and impregnated samples,

348   which reveals that the proportion of each copper species on the surface is only

349   influenced by the copper amount and the zeolite type.

350   Additional information about the nature of the different copper species in the

351   catalysts was obtained by Temperature Programmed Reduction experiments (H_2-TPR),

352   and Figure 6 shows the H_2 consumption profiles. The copper-free H-zeolites did not

353   contain reducible ions and no H_2 consumption was noticed; therefore, all H_2 consumed

354   by the catalysts can be attributed to the reduction of copper cations. It is important to

355   mention that the H_2-TPR profiles obtained with fresh catalysts (Figure 6) and after the

356   SCR experiments (not shown) did not show significant changes, confirming that copper

357   remains mainly oxidized even after the SCR experiments. This is not surprising taking

358   into account the highly oxidizing nature of the simulated diesel exhaust gas stream.

359   FIGURE 6

360   All the catalysts consumed H_2 due to the reduction of Cu(II), and the higher the

361   copper content of the catalysts, the higher the H_2 consumption [30]. Considering the

14

362   ICP-AES copper content, the amount of catalyst used in the H_2-TPR experiments and

363   the stoichiometry of the following reactions:

364    $CuO + H_2 \rightarrow Cu + H_2O$ (for bulk CuO particles)   (6)

365    $Cu(II)\text{-}zeolite + H_2 \rightarrow Cu + (2H^+)\text{-}zeolite$ (for Cu(II) cations exhanged on the zeolites)(7)

366   a $H_2/Cu=1$ ratio should be obtained if all copper were Cu(II) and if all Cu(II) species

367   were completely reduced to metal copper. According to the H_2/Cu ratios obtained

368   experimentally (0.9-1.0 in all cases), all the catalysts accomplish these hypotheses.

369   This confirms that only Cu(II) species exist on the catalysts, which is consistent with the

370   XPS results.

371   All the profiles included in Figure 6 are composed by several maxima and

372   shoulders indicating, in line with the XSP results, the presence of copper species with

373   different reducibility. The maximum that appears around 250 °C for most of the

374   catalysts corresponds to the reduction of bulk CuO species, which are more easily

375   reduced than exchanged Cu(II) ions [31]. A shoulder at lower temperatures, which is

376   related with the reduction of the CuO particles surface, is observed in some profiles,

377   and its contribution increases with the total copper content. The CuO reduction

378   maximum/shoulder observed in the H_2-TPR profiles would be associated to the copper

379   2p XPS contribution at 933.2 eV (see Figure 5 and Table 3).

380   The H_2-consumption peaks appearing at higher temperatures can be assigned

381   to Cu(II) cations exchanged on the zeolite, which need more temperature to be

382   reduced than CuO. The presence of different exchanged Cu(II) cations is consequence

383   of the existence of different kinds of framework sites in ZSM5 and BETA zeolites [29].

384   The peaks with a maximum at temperatures around 350 °C for ZSM5 catalysts and

385   around 450 °C for BETA catalyst, corresponds to the most easily reduced exchanged

386   Cu (II) species [31]. According to the XPS results, this peak could be related with the

387 reduction of tetracoordinated Cu(II) species. Finally, the peaks with a maximum at

388 temperatures around 480 °C for ZSM5 catalysts and around 600 °C for BETA catalysts

389 correspond, in line with XPS results, to the reduction of Cu(II) cations in octahedral

390 coordination, which are strongly attached to the zeolite.

391   As it has been previously reported [30], there is a significant effect of copper

392 loading on the reducibility of the different copper species. From our data it can be

393 confirmed that an increase of the copper loading shifts the reduction peaks to lower

394 temperature. This is consistent with the formation of larger amounts of dimeric copper-

395 species as the copper loading increases [32]. These dimeric copper species contain

396 bridging oxygen atoms that can react with H_2 at comparably lower temperatures than

397 isolated copper-sites. Thus, as expected, the copper dispersion decreases for high

398 copper loading.

399   In addition to the qualitative assignation of the H_2-reduction peaks to the

400 different copper species in the catalyst, a semi-quantitative analysis of the H_2-

401 consumption profiles can be done. The highest temperature peaks (assigned to Cu(II)

402 cations exchanged on octahedral sites) are the most intense peaks for the low copper

403 content catalysts. This indicates that the octahedral sites are first exchanged. The

404 intensity of the peaks assigned to Cu(II) cations exchanged on tetrahedral sites grows

405 appreciably with the copper content, becoming more intense than the third contribution

406 (the one assigned to Cu(II) cations exchanged on octahedral sites). This confirms that

407 the tetra-coordinated sites are occupied by Cu(II) cations after the octahedral sites, and

408 that the amount of tetrahedral sites available on the zeolites is higher to that of

409 octahedral sites. Finally, the most intense H_2-reduction peak of the ZSM5 catalyst with

410 highest copper content (Z-IE-4.9) is assigned to CuO reduction, confirming that bulk

411 copper oxide formation is favored once the exchange sites have been occupied. On the

412 contrary, the position and intensity of the H_2-reduction peaks of B-IE-5.8 suggest that

413 Cu(II) exchanged on tetrahedral positions is the most abundant copper species on the

414 highest copper content BETA catalyst. This is consistent with the lower Si/Al ratio, and

415 therefore higher ionic exchange capacity, of the BETA zeolite with regard to that of the

416 ZSM5 zeolite, and to the more accessible porosity of the BETA zeolite.

417 As a summary, the XPS and H_2-TPR characterization confirm the presence of

418 different Cu(II) species on the catalyst, namely, CuO and Cu(II) exchanged on

419 tetrahedral and octahedral positions of the zeolite framework. Clear evidences of Cu(I)

420 or Cu(0) species were not obtained in any case. As a general trend, Cu(II) exchanged

421 on octahedral positions prevails for catalysts with low copper content, and the

422 exchange of Cu(II) on tetrahedral positions and the formation of CuO is progressively

423 favored by increasing the copper content. The formation of CuO is more important on

424 the ZSM5 zeolite than on BETA due to the higher Si/Al ratio, and therefore lower ionic

425 exchange capacity, of the former, and to the more accessible porosity of the BETA

426 zeolite.

427

428 *3.4. SCR experiments.*

429 Figures 7a and 7b show the NO_x and NH_3 conversions and Figures 7c, 7d and

430 7e show the selectivity towards N_2, NO_2 and N_2O, respectively, as a function of the

431 reaction temperature in SCR experiments.

432 FIGURE 7

433 The behavior of any catalyst is qualitatively similar, and the obtained catalytic

434 results are typical of NO_x SCR reactions in all cases. NO conversions increased with

435 temperature because the NH_3-NO_x reactions are promoted, reaching a maximum

436 conversion for an intermediate temperature and decreasing afterwards as the oxidation

437 of ammonia with O_2 is favored at high temperature [33, 34]. The NH_3 conversions also

17

438   increased with temperature, but 100% conversion was maintained above a certain

439   temperature because the NH_3-O_2 reaction prevails. The minimum temperature for

440   100% ammonia conversion is the same at which the maximum NO conversion is

441   achieved. Regardless the catalyst, N_2 is the main nitrogen-reaction product (above

442   80% selectivity in the whole range of temperatures studied for all catalyst) and few N_2O

443   and/or NO_2 are only detected.

444   The particular behavior of the catalysts depends on the zeolite nature, on the

445   copper content and on the copper loading procedure. The lowest NOx conversions

446   were obtained with the impregnated catalysts, and this could be a consequence of the

447   partial blockage of the zeolite network by copper species, as deduced from the BET

448   values (see Figure 2). The partial blockage of the zeolite pores is expected to force the

449   reactions to preferentially occur on the external surface of the crystals, hindering the

450   access of gases to the internal copper sites.

451   For catalysts prepared with the same zeolite, the NO and NH_3 conversion

452   curves are shifted to lower temperatures as the copper content increases, while the

453   N_2O and NO_2 selectivities slightly increase. As discussed in the previous

454   characterization sections, the presence of CuO is favored for high copper contents, and

455   this would explain these catalytic trends. A tentative explanation is that CuO catalyzes

456   the oxidation of NO to NO_2, and this favors the reduction of NO_x at lower temperature

457   since the NH_3-NO_2 reaction is faster than the NH_3–NO reaction (NO_2 is much more

458   oxidizing than NO). The formation of NO_2 is only evident at high temperature, once the

459   selectivity of the NH_3-NO_x reactions decrease, because in the range of temperatures of

460   high NO reduction selectivity the NO_2 potentially formed is expected to react with NH_3,

461   and consequently, is not detected.

462   The low-copper content catalysts, and mainly those prepared by ionic exchange

463   and with BETA zeolite, have a better catalytic behavior at high temperature than the

464   high-copper content counterparts. For instance, at 425 °C, the catalyst B-IE-2.1

465   reached the highest NO conversion among all catalysts, keeping low NO_2 and N_2O

466   production. This catalyst has a high proportion of exchanged Cu(II) species (mainly

467   Cu(II) exchanged on octahedral sites), and this type of copper cations seems to be

468   responsible of the activity at high temperature. It can be concluded that CuO clusters,

469   which are more abundant in high copper-content catalysts, promote NO reduction at

470   low temperature whereas isolated Cu(II) ions, which are more abundant in low copper-

471   content catalysts, maintained high NO_x conversion even at high temperatures. In

472   addition, catalysts with low CuO content exhibit higher N_2 selectivity, which was

473   progressively reduced by increasing the copper loading. In those cases, the selectivity

474   of the reaction moved towards N_2O and NO_2.

475   Comparing the supports, it can be observed that Cu-ZSM5 catalysts are more

476   active at low temperature whereas Cu-BETA catalysts maintain higher activity at high

477   temperature. This behavior can also be related to the nature of the copper species

478   present in each catalyst. As a general trend, there are higher amounts of CuO on

479   ZSM5 catalysts than on BETA catalysts due to the higher Si/Al ratio, and therefore

480   lower ionic exchange capacity, of the ZSM5 zeolite, and to the more accessible

481   porosity of the BETA zeolite, which favors the formation of exchanged Cu(II) species

482   with regard to bulk CuO particles.

483   **4. Conclusions.**

484   In this study, the SCR of NO_x with NH_3 has been studied with different copper

485   zeolite catalysts and the following conclusions have been achieved:

486   The catalysts characterization confirmed the presence of different Cu(II) species

487   in all catalyst, namely, CuO and Cu(II) exchanged on tetrahedral and octahedral

488   positions of the zeolite framework. Clear evidences of Cu(I) or Cu(0) species were not

489   obtained in any case. As a general trend, Cu(II) exchanged on octahedral positions

490   prevails for catalysts with low copper content, and the exchange of Cu(II) on tetrahedral

491   positions and the formation of CuO is progressively favored by increasing the copper

492   content.

493   CuO is more abundant in high copper-content catalysts and in ZSM5 catalysts,

494   while isolated Cu(II) ions are more abundant in low copper-content catalysts and in

495   BETA catalysts. There are higher amounts of CuO on ZSM5 catalysts than on BETA

496   catalysts due to the lower ionic exchange capacity of the ZSM5 zeolite.

497   The nature of the copper species affects the SCR behavior of the studied

498   catalysts. CuO clusters promote NO reduction at low temperature whereas isolated

499   Cu(II) ions maintain high NO_x conversion at high temperatures. In addition, catalysts

500   with low CuO content exhibit higher N_2 selectivity, since CuO promotes the formation of

501   N_2O and NO_2.

502   It is suggested that CuO catalyzes the oxidation of NO to NO_2, and this favors

503   the reduction of NO_x at lower temperature since the NH_3-NO_2 reaction is faster than the

504   NH_3–NO reaction (NO_2 is much more oxidizing than NO).

505

506

513   **REFERENCES**

514   [1]   P. Forzatti, L. Lietti, E. Tronconi, Nitrogen Oxides Removal Industrial, in:
515   Encyclopedia of Catalysis, John Wiley & Sons, Inc., 2002.

516   [2]   R.M. Heck, R.J. Farrauto, S.T. Gulati, Diesel Engine Emissions, in:
517   Catalytic Air Pollution Control, John Wiley & Sons, Inc., 2009, pp. 238-
518   294.

519   [3]   P. Forzatti, L. Lietti, I. Nova, E. Tronconi, Diesel NOx aftertreatment
520   catalytic technologies: Analogies in LNT and SCR catalytic chemistry,
521   Catalysis Today. 151 (2010) 202-211.

522   [4]   L. Lietti, I. Nova, E. Tronconi, P. Forzatti, Transient kinetic study of the
523   SCR-DeNOx reaction, Catalysis Today. 45 (1998) 85-92.

524   [5]   E.C. Corbos, M. Haneda, X. Courtois, P. Marecot, D. Duprez, H.
525   Hamada, Cooperative effect of Pt–Rh/Ba/Al and CuZSM-5 catalysts for
526   NOx reduction during periodic lean-rich atmosphere, Catalysis
527   Communications. 10 (2008) 137-141.

528   [6]   N. Wilken, K. Wijayanti, K. Kamasamudram, N.W. Currier, R. Vedaiyan,
529   A. Yezerets, L. Olsson, Mechanistic investigation of hydrothermal aging
530   of Cu-Beta for ammonia SCR, Applied Catalysis B: Environmental. 111–
531   112 (2012) 58-66.

532   [7]   A. Corma, V. Forne´s, E. Palomares, Selective catalytic reduction of NOx
533   on Cu-beta zeolites, Applied Catalysis B: Environmental. 11 (1997) 233-
534   242.

535   [8]   S. T. Korhonen, D. W. Fickel, R. F. Lobo, B. M. Weckhuysen, A. M.
536   Beale, Chemical Communications. 47 (2011), 800-802.

537   [9]   S. J. Schmieg, S. H. Oha, C. H. Kima, D. B. Brown, J. H. Lee, C. H.F.
538   Peden, D. H. Kim. Catalysis Today 184 (2012) 252– 261.

539   [10]   A. Grossale, I. Nova, E. Tronconi, D. Chatterjee, M. Weibel, The
540   chemistry of the NO/NO2–NH3 "fast" SCR reaction over Fe-ZSM5
541   investigated by transient reaction analysis, Journal of Catalysis. 256
542   (2008) 312-322.

543   [11]   S. Brandenberger, O. Kroecher, A. Tissler, R. Althoff, The State of the
544   Art in Selective Catalytic Reduction of NOx by Ammonia Using Metal-
545   Exchanged Zeolite Catalysts, Catalysis Reviews-Science and
546   Engineering. 50 (2008) 492-531.

547   [12]   R. Burch, P.J. Millington, Role of propene in the selective reduction of
548   nitrogen monoxide in copper-exchanged zeolites, Applied Catalysis B:
549   Environmental. 2 (1993) 101-116.

550   [13]   G.D. Lei, B.J. Adelman, J. Sárkány, W.M.H. Sachtler, Identification of
551   copper(II) and copper(I) and their interconversion in Cu/ZSM-5 De-NOx
552   catalysts, Applied Catalysis B: Environmental. 5 (1995) 245-256.

553   [14]   R. Pirone, P. Ciambelli, G. Moretti, G. Russo, Nitric oxide decomposition
554   over Cu-exchanged ZSM-5 with high Si/Al ratio, Applied Catalysis B:
555   Environmental. 8 (1996) 197-207.

556   [15]   B. Modén, P. Da Costa, B. Fonfé, D.K. Lee, E. Iglesia, Kinetics and
557   Mechanism of Steady-State Catalytic NO Decomposition Reactions on
558   Cu–ZSM5, Journal of Catalysis. 209 (2002) 75-86.

559   [16]   J. Dědeček, L. Čapek, B. Wichterlová, Nature of active sites in decane-
560   SCR-NOx and NO decomposition over Cu-ZSM-5 zeolites, Applied
561   Catalysis A: General. 307 (2006) 156-164.

562   [17]   G. Moretti, C. Dossi, A. Fusi, S. Recchia, R. Psaro, A comparison
563   between Cu-ZSM-5, Cu–S-1 and Cu–mesoporous-silica–alumina as
564   catalysts for NO decomposition, Applied Catalysis B: Environmental. 20
565   (1999) 67-73.

566   [18]   U. De La Torre, B. Pereda-Ayo, J.R. González-Velasco, Cu-zeolite NH3-
567   SCR catalysts for NOx removal in the combined NSR–SCR technology,
568   Chem. Eng. J. 207–208 (2012) 10-17.

569   [19]   V.I. Pârvulescu, P. Grange, B. Delmon, NO decomposition over physical
570   mixtures of Cu-ZSM-5 with zeolites or oxides, Applied Catalysis B:
571   Environmental. 33 (2001) 223-237.

572   [20]   V.K. Kaushik, R.P. Vijayalakshmi, N.V. Choudary, S.G.T. Bhat, XPS
573   studies on cation exchanged zeolite A, Microporous and Mesoporous
574   Materials. 51 (2002) 139-144.

[21]   L.O. Öhman, B. Ganemi, E. Björnbom, K. Rahkamaa, R.L. Keiski, J. Paul, Catalyst preparation through ion-exchange of zeolite Cu-, Ni-, Pd-, CuNi- and CuPd-ZSM-5, Mater. Chem. Phys. 73 (2002) 263-267.

[22]   G. Centi, S. Perathoner, Nature of active species in copper-based catalysts and their chemistry of transformation of nitrogen oxides, Applied Catalysis A: General. 132 (1995) 179-259.

[23]   B.M. Abu-Zied, Cu2+-acetate exchanged X zeolites: Preparation, characterization and N2O decomposition activity, Microporous and Mesoporous Materials. 139 (2011) 59-66.

[24]   http://www.iza-online.org/ Access on August 2013.

[25]   A. Corma, A. Palomares, F. Márquez, Determining the Nature of the Active Sites of Cu-Beta Zeolites for the Selective Catalytic Reduction (SCR) of NOx by Using a Coupled Reaction-XAES/XPS Study, Journal of Catalysis. 170 (1997) 132-139.

[26]   www.lasurface.com, accessed on 7th May 2013.

[27]   M. Fernández-García, E. Gómez Rebollo, A. Guerrero Ruiz, J.C. Conesa, J. Soria, Influence of Ceria on the Dispersion and Reduction/Oxidation Behaviour of Alumina-Supported Copper Catalysts, Journal of Catalysis. 172 (1997) 146-159.

[28]   J.F. Xu, W. Ji, Z.X. Shen, S.H. Tang, X.R. Ye, D.Z. Jia, X.Q. Xin, Preparation and Characterization of CuO Nanocrystals, Journal of Solid State Chemistry. 147 (1999) 516-519.

[29]   R. Hajjar, Y. Millot, P.P. Man, M. Che, S. Dzwigaj, Two Kinds of Framework Al Sites Studied in BEA Zeolite by X-ray Diffraction, Fourier Transform Infrared Spectroscopy, NMR Techniques, and V Probe, Journal of Physical Chemistry C. 112 (2008) 20167-20175.

[30]   B. Moden, J.M. Donohue, W.E. Cormier, H.-. Li, Effect of Cu-loading and structure on the activity of Cu-exchanged zeolites for NH3-SCR, in: Studies in Surface Science and Catalysis, Elsevier, pp. 1219-1222.

[31]   J. Zhou, Q.-. Xia, S.-. Shen, S. Kawi, K. Hidajat, Catalytic oxidation of pyridine on the supported copper catalysts in the presence of excess oxygen, Journal of Catalysis. 225 (2004) 128-137.

[32]   P. Da Costa, B. Moden, G. Meitzner, D. Lee, E. Iglesia, Spectroscopic and chemical characterization of active and inactive Cu species in NO decomposition catalysts based on Cu-ZSM5, Physical Chemistry Chemical Physics. 4 (2002) 4590-4601.

611   [33] J.H. Kwak, D. Tran, S.D. Burton, J. Szanyi, J.H. Lee, C.H.F. Peden,
612   Effects of hydrothermal aging on NH3-SCR reaction over Cu/zeolites,
613   Journal of Catalysis. 287 (2012) 203-209.

614   [34] J. Li, H. Chang, L. Ma, J. Hao, R.T. Yang, Low-temperature selective
615   catalytic reduction of NOx with NH3 over metal oxide and zeolite
616   catalysts—A review, Catalysis Today. 175 (2011) 147-156.

617

618   **Figure Captions.**

619
620
621   **Figure 1.**   Relation between the initial copper concentration and the actual copper
622   content (%) in zeolite.
623
624   **Figure 2.**   Relation between the actual copper content and BET surface area.
625
626   **Figure 3.**   TEM images of (a) Z-IE-1.4, (b) Z-IE-4.9, (c) B-IE-2.1 and (d) B-IE-5.8.
627
628   **Figure 4.**   Particle size distribution of catalysts determined from TEM images.
629
630   **Figure 5.**   X ray Photoelectric Spectra (copper $2p^{3/2}$ transition) for (a) Cu-ZSM5
631   catalysts and (b) Cu-BETA catalysts.
632
633   **Figure 6.** H_2-TPR profiles of fresh: a) Cu-BETA catalysts and (b) Cu-ZSM-5 catalysts.
634
635   **Figure 7.**   Conversion of NO_x, NH_3 and N_2, N_2O and NO_2 selectivity during SCR
636   reaction for (a) BETA and (b) ZSM5 catalysts.

637

638

639 **Table 1.** Summary of the prepared catalysts

Catalyst nomenclature	Support	Si/Al	Copper loading method	Copper initial concentration in the impregnation solutions (ppm)	Copper content on the catalyst (wt. %)	Exchange sites potentially* occupied by Cu(II) cations (%)
B-IM-1.3	BETA	12.5	Impregnation	-	1.3	23
B-IE-2.1	BETA	12.5	Ion exchange	320	2.1	37
B-IE-2.9	BETA	12.5	Ion exchange	640	2.9	52
B-IE-5.8	BETA	12.5	Ion exchange	2000	5.8	103
Z-IM-1.2	ZSM5	25	Impregnation	-	1.2	59
Z-IE-1.4	ZSM5	25	Ion exchange	160	1.4	69
Z-IE-2.6	ZSM5	25	Ion exchange	640	2.6	129
Z-IE-4.9	ZSM5	25	Ion exchange	2000	4.9	243

640

641

642   **Table 2.** Results of the surface characterization by XPS.

Catalyst	$Cu_{surface}/Cu_{total}$	Si/Al
Z-IM-1.2	0.78	14
Z-IE-1.4	0.38	14
Z-IE-2.6	0.58	8
Z-IE-4.9	0.64	5
B-IM-1.3	0.37	11
B-IE-2.1	0.42	8
B-IE-2.9	0.42	7
B-IE-5.8	0.42	6

643

644

645

646   **Table 3.** XPS characterization of the copper species. Percentage of the different
647   copper species identified in the $Cu2p^{3/2}$ transition and Auger energy.

Catalyst	Peak at 933.2 eV (%)	Peak at 934.0 eV (%)	Peak at 936.0 eV (%)	Auger (eV)
Z-IM-1.2	9	83	8	1865.3
Z-IE-1.4	13	78	8	1865.6
Z-IE-2.6	31	59	10	1865.2
Z-IE-4.9	53	38	9	1848.6
B-IM-1.3	9	79	12	1865.6
B-IE-2.1	16	74	10	1865.5
B-IE-2.9	27	57	16	1865.9
B-IE-5.8	34	45	21	1862.3

648   Tentative assignation: 933.2 eV corresponds to CuO, 934.0 eV corresponds to isolated Cu(II) in
649   tetrahedral coordination and 936.0 eV corresponds to isolated Cu(II) in octahedrical
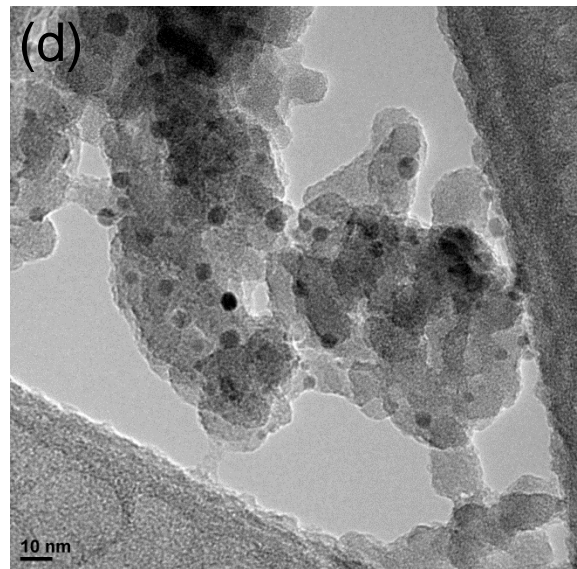650   coordination (see main text for details).
651
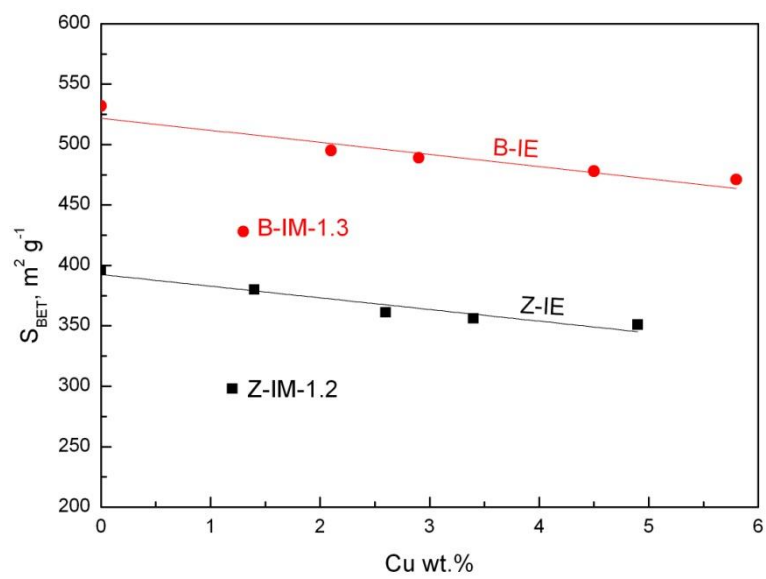
652

Figure 1

653

654

655

656   **Figure 2**

657
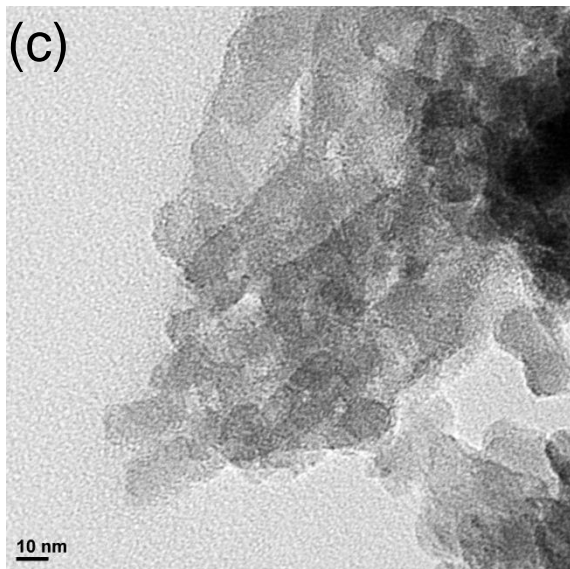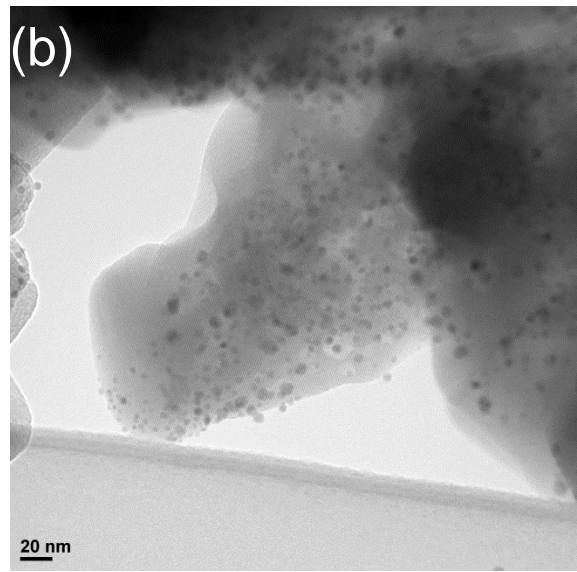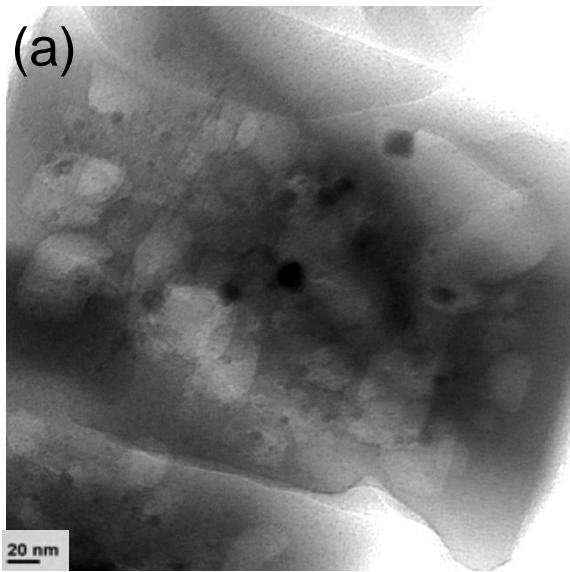
(a)

20 nm

(b)

20 nm

(c)

10 nm

(d)

10 nm

658

659   **Figure 3**

660

661

662

Figure 4

663

664

665

(a)

I, a.u.

Z-IE-4.9

Z-IE-2.6

Z-IE-1.4

Z-IM-1.2

930   932   934   936   938   940

Binding E, eV

(b)

I, a.u.

B-IE-5.8

B-IE-2.9

B-IE-2.1

B-IM-1.3

930   932   934   936   938   940

Binding E, eV

666

667

668   **Figure 5**

669

670

671

672
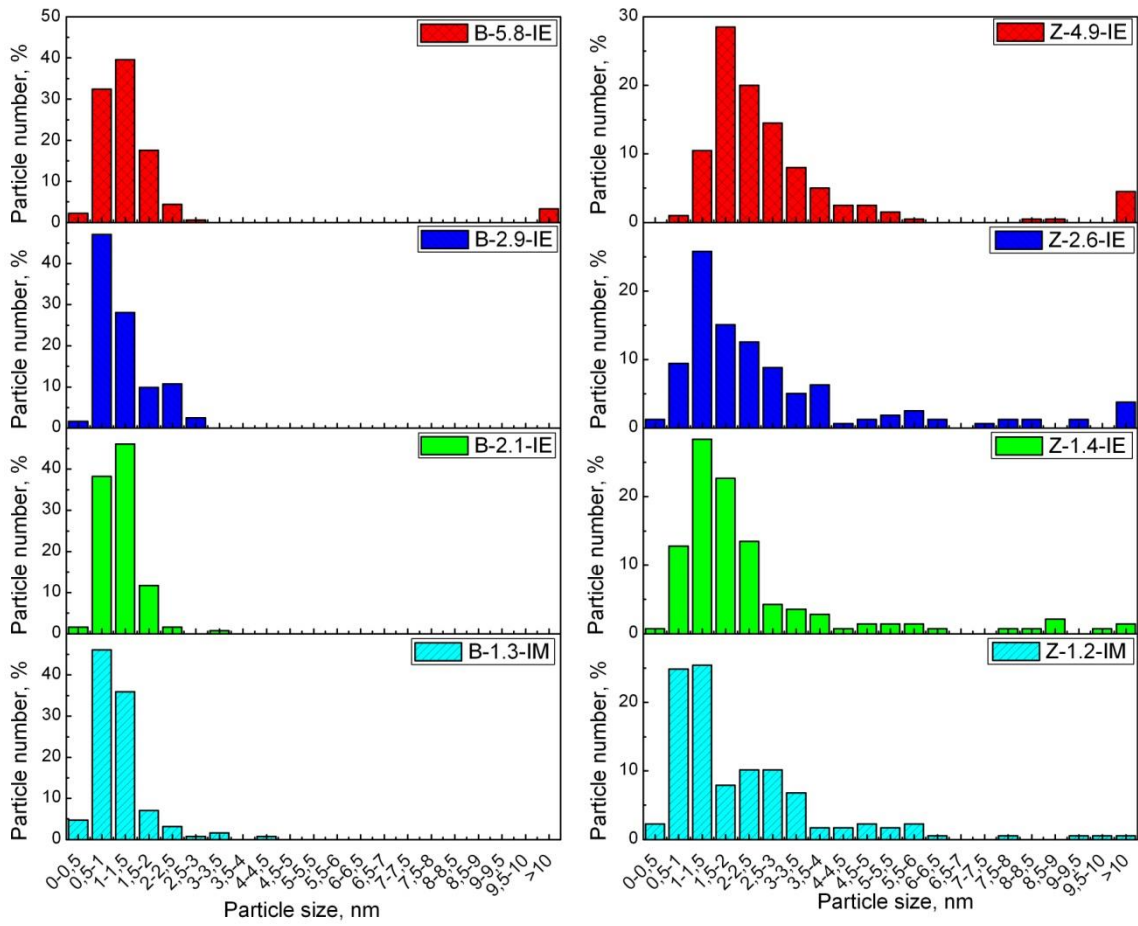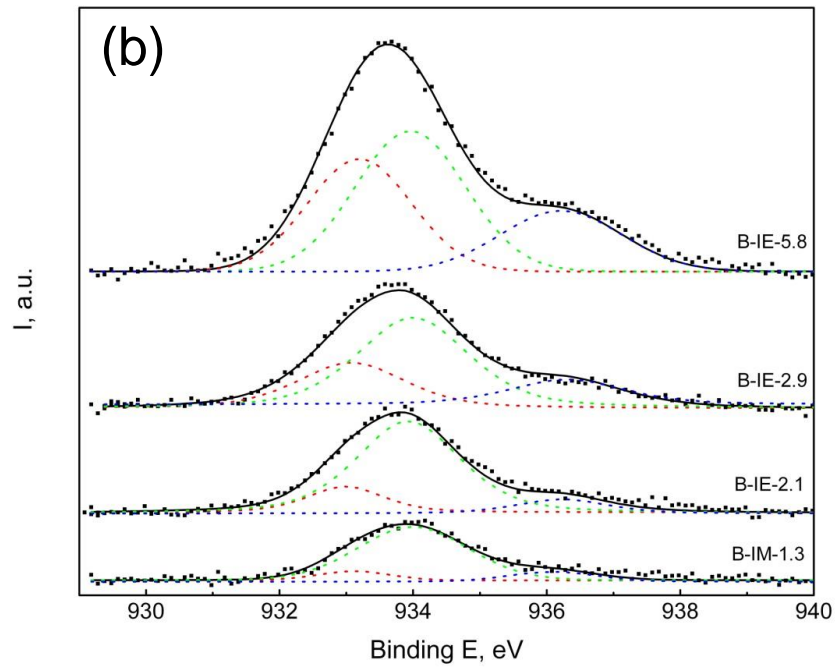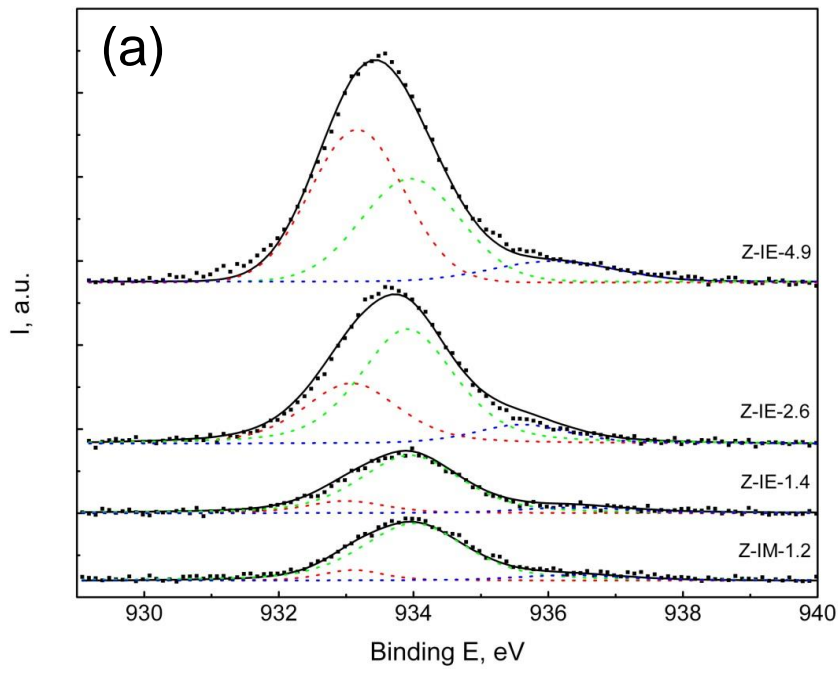
Figure 6
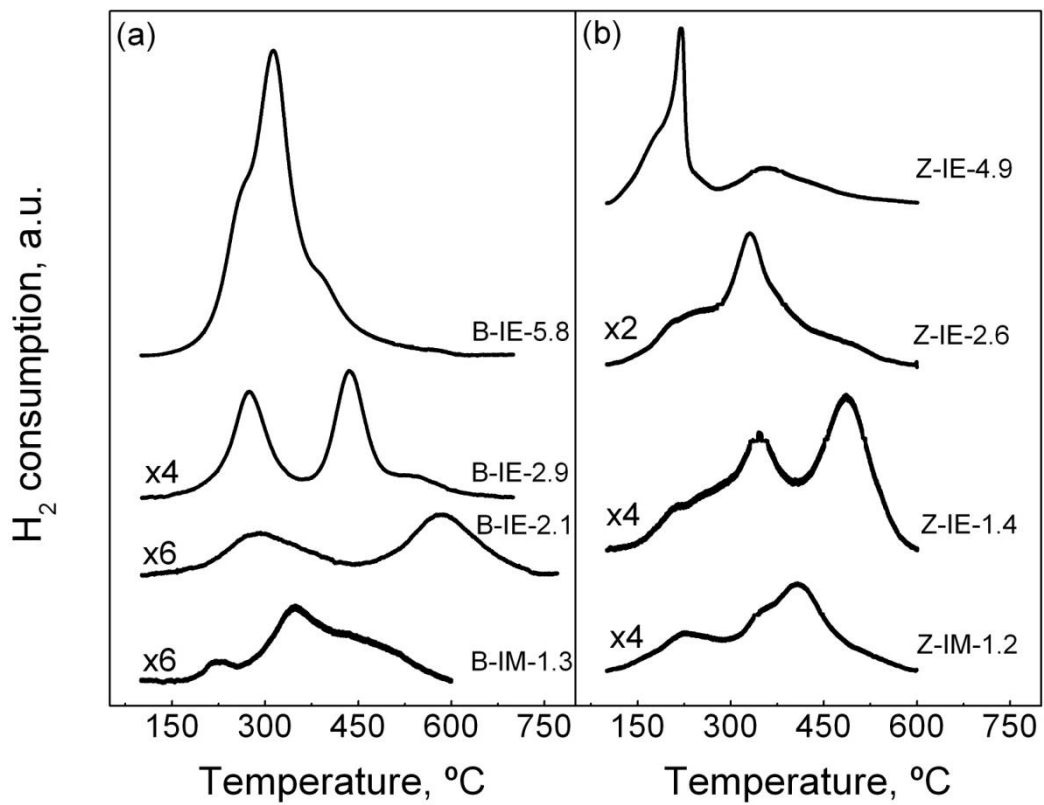
677

678

679   **Figure 7**